Gate-induced Dirac cones in multilayer graphenes

Takahiro Morimoto[1] and Mikito Koshino[2]
[1]*Condensed Matter Theory Laboratory, RIKEN, Saitama 351-0198, Japan*
[2]*Department of Physics, Tohoku University, Sendai 980-8578, Japan*
(Received 30 November 2012; published 19 February 2013)

We study the electronic structures of ABA (Bernal) -stacked multilayer graphenes in a uniform perpendicular electric field, and we show that the interplay of the trigonal warping and the potential asymmetry gives rise to a number of emergent Dirac cones nearly touching at zero energy. The band velocity and the energy region (typically a few tens of meV) of these gate-induced Dirac cones are tunable with the external electric field. In ABA-trilayer graphene, in particular, applying an electric field induces a nontrivial valley Hall state, where the energy gap at the Dirac point is filled by chiral edge modes which propagate in opposite directions between two valleys. In four-layer graphene, in contrast, the valley Hall conductivity is zero and there are no edge modes filling in the gap. A nontrivial valley Hall state generally occurs in asymmetric odd-layer graphenes, and this is closely related to a hidden chiral symmetry which exists only in odd-layer graphenes.

DOI: 10.1103/PhysRevB.87.085424 PACS number(s): 73.22.Pr, 81.05.ue, 73.43.Cd

I. INTRODUCTION

Graphene is characterized with Dirac quasiparticles in the low-energy region,[1–4] which give rise to anomalous physical properties due to the linear dispersion and nontrivial Berry phase.[5–11] There are growing interests in multilayer variants of graphene such as bilayers[12–15] and trilayers,[16–20] which also support chiral quasiparticles. Bilayer graphene has parabolic valence and conduction bands touching each other at the Dirac point,[21–23] while ABA (Bernal) -stacked trilayer graphene comes with a superposition of effective monolayer-like and bilayer-like bands.[22,24–32]In addition to these, the trigonal-warping deformation of the energy band, which is intrinsic to graphite-based systems,[33–35] gives rise to small Dirac cones near the Dirac point in these multilayers. The Lifshitz transition, in which the Fermi circle breaks up into separate parts, takes place at a small energy scale around a few meV.[21,23,28–30]

On the other hand, it is possible to modify the band structure of multilayer graphenes by applying an electric field perpendicular to the layer, using external gate electrodes attached to the graphene sample. In bilayer graphene, a perpendicular electric field opens a band gap at the Dirac point.[13,15,21,22,26,36–38] In contrast, for ABA-trilayer graphene, previous works[30,39] considered the gate-field effect on the band structure without the trigonal warping, and they showed that the perpendicular electric field causes a band overlap of the conduction and valence bands at zero energy, rather than opening a gap. These two bands intersect on a circle around the K point whose radius is proportional to the potential asymmetry, causing an increase of the conductivity at the charge neutral point.[17]

In this paper, we closely study the band structures of ABA-stacked multilayer graphenes in the presence of a uniform perpendicular electric field, and we find that the interplay of the trigonal warping and the potential asymmetry generally gives rise to a number of additional Dirac cones nearly touching at zero energy, as depicted in Fig. 1(b) for trilayer graphene. For these gate-induced Dirac cones, the band velocity and the energy region (i.e., the distance between the Dirac point to the Lifshitz transition point) are tunable with gate bias voltage. The energy region is typically a few tens of meV, which is greater by an order of magnitude than in the original nonbiased multilayer graphene. In a magnetic field, there arise triply degenerate Landau levels originating from off-center gate-induced Dirac cones, with wide energy spacings due to the linear dispersion.

The gate-induced Dirac cones are generally gapped at the Dirac point by symmetry-breaking terms. When the Fermi energy is in the gap, the system is in a topologically nontrivial valley Hall state, where electrons at K_+ and K_- valleys carry opposite Hall conductivities.[40,41] A manifestation of the valley Hall state is the emergence of chiral edge modes at a zigzag interface which transports valley pseudospins in an analogous way to the spin Hall effect.[42,43] The valley Hall state and the helical edge modes were previously studied for gapped monolayer and bilayer graphenes,[40,44–48] and also for ABC (rhombohedral) -stacked trilayer graphene.[49] We study the edge states a semi-infinite zigzag ribbon of asymmetric ABA multilayer graphenes, and we relate the number of edge modes to the valley Hall conductivity which is a bulk property. In trilayer graphene, in particular, we find that the nonzero valley Hall state is realized in a small external electric field, and moreover, a topological transition takes place at a certain higher electric field, which is accompanied by a change of the number of edge channels inside the bulk gap. In four-layer graphene, in contrast, the valley Hall conductivity is always zero and there are no edge modes filling the energy gap. We show that the nontrivial valley Hall state generally occurs in asymmetric odd-layer graphenes, and this is largely due to an approximate chiral symmetry peculiar to odd-layer graphenes.

This paper is organized as follows. We briefly introduce the effective-mass model for graphite in Sec. II, and we discuss the trilayer graphene in Sec. III in terms of the gate-induced Dirac cones, the chiral symmetry, the Landau-level structure, and the edge states. In Sec. IV, we study the four-layer graphene as an example of even-layer cases without chiral symmetry. In Sec. V, we discuss the chiral symmetry in general odd-layer graphenes, generalizing the trilayer's argument. The conclusion is given in Sec. VI.

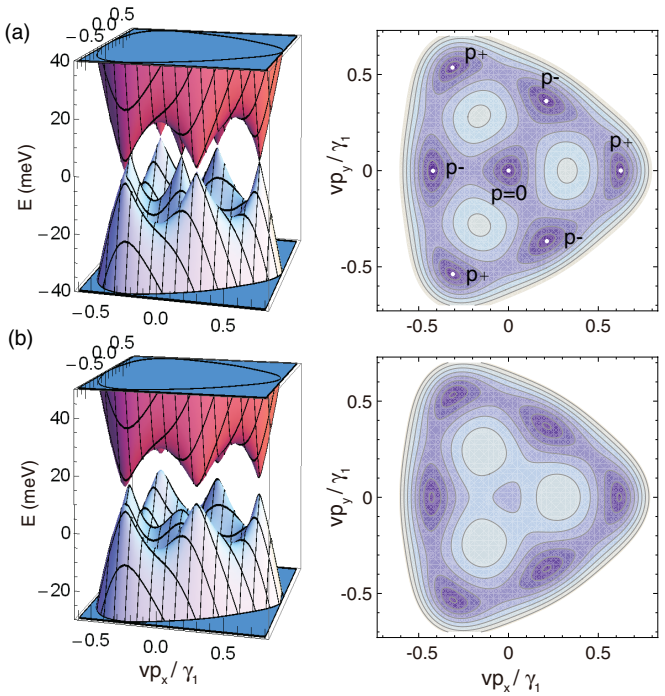

FIG. 1. (Color online) Band structures of ABA-trilayer graphene in a perpendicular electric field depicted in a three-dimensional (3D) plot (left panel) and contour plot (right), for the band models (a) only with v, γ_1, v_3 terms and (b) with full parameters. The interlayer potential asymmetry is set to be $\Delta = 200$ meV.

II. MODEL

We describe the electronic properties of ABA-stacked multilayer graphene using the Slonczewski-Weiss-McClure model[33–35] with hopping parameters described in Fig. 2. The model includes intralayer coupling γ_0, nearest interlayer couplings γ_1, γ_3, and γ_4, next-nearest layer couplings γ_2 and γ_5, and on-site energy asymmetry Δ', which are estimated in bulk graphite as follows:[35] $\gamma_0 = 3.16$ eV, $\gamma_1 = 0.39$ eV, $\gamma_3 = 0.32$ eV, $\gamma_2 = -0.020$ eV, $\gamma_5 = 0.038$ eV, $\gamma_4 = 0.044$ eV, and $\Delta' = 0.050$ eV. Δ' is the energy difference between the sites which are involved in the coupling γ_1 and the sites which are not.

We consider ABA-stacked N-layer graphene, where $|A_j\rangle$ and $|B_j\rangle$ represent Bloch functions at the K_ξ point, corresponding to the A and B sublattices of layer j, respectively. If the basis is arranged as $|A_1\rangle, |B_1\rangle; |A_2\rangle, |B_2\rangle; \ldots; |A_N\rangle, |B_N\rangle$, the Hamiltonian in the vicinity of the K_ξ valley is written as[22,25,28,29]

$$\mathcal{H} = \begin{pmatrix} H_0 & V & W & & & \\ V^\dagger & H_0' & V^\dagger & W' & & \\ W & V & H_0 & V & W & \\ & W' & V^\dagger & H_0' & V^\dagger & W' \\ & & \ddots & \ddots & \ddots & \end{pmatrix} + \begin{pmatrix} U_1 & & & & & \\ & U_2 & & & & \\ & & U_3 & & & \\ & & & U_4 & & \\ & & & & \ddots & \end{pmatrix} \quad (1)$$

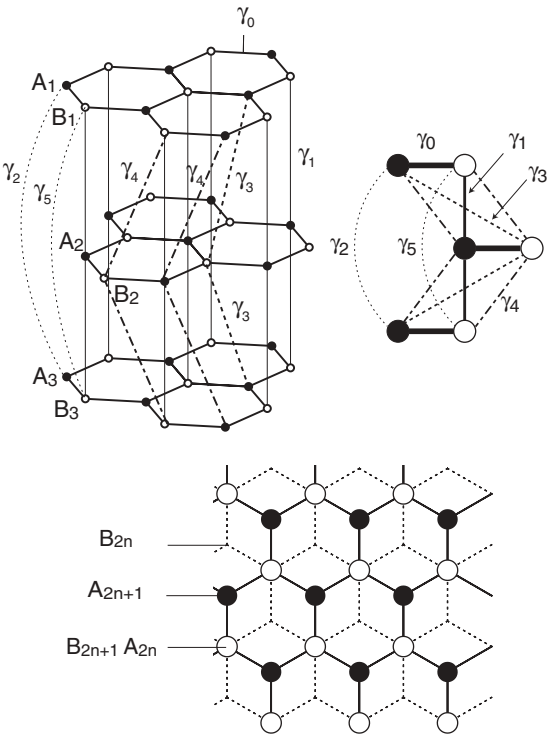

FIG. 2. Lattice structure of ABA-trilayer graphene with tight-binding hopping parameters. The bottom figure is a top view, and the right is a schematic diagram of the lattice structure.

with

$$H_0 = \begin{pmatrix} 0 & v\pi^\dagger \\ v\pi & \Delta' \end{pmatrix}, \quad H_0' = \begin{pmatrix} \Delta' & v\pi^\dagger \\ v\pi & 0 \end{pmatrix},$$
$$V = \begin{pmatrix} -v_4\pi^\dagger & v_3\pi \\ \gamma_1 & -v_4\pi^\dagger \end{pmatrix},$$
$$W = \begin{pmatrix} \gamma_2/2 & 0 \\ 0 & \gamma_5/2 \end{pmatrix}, \quad W' = \begin{pmatrix} \gamma_5/2 & 0 \\ 0 & \gamma_2/2 \end{pmatrix},$$
$$U_j = -\Delta\left(j - \frac{N+1}{2}\right)\begin{pmatrix} 1 & 0 \\ 0 & 1 \end{pmatrix},$$

where $\pi = \xi\pi_x + i\pi_y$, $\boldsymbol{\pi} = \boldsymbol{p} + e\boldsymbol{A}$, with $\boldsymbol{A}$ being the vector potential arising from the applied magnetic field, and $\xi = \pm 1$ are the valley indices for $K_\pm$. The parameter $v = \sqrt{3}a\gamma_0/(2\hbar)$ is the band velocity for monolayer graphene, and $v_3 = \sqrt{3}a\gamma_3/(2\hbar)$ is a velocity related to the band parameter γ_3, where $a \approx 0.246$ nm is the distance between the nearest A sites on the same layer. U_j describes the electrostatic potential on the jth layer induced by the external electric field, where we assumed a uniform potential gradient in the perpendicular direction, This is valid in a few-layer graphene with typically $N < \sim 5$. For thicker multilayers with $N > \sim 10$, the potential drop occurs within a few layers near the external gate due to the screening by the charge carriers in graphene.[30,39]

III. TRILAYER GRAPHENE

A. Chiral symmetry and gate-induced Dirac cones

The Hamiltonian of ABA-trilayer graphene is given by Eq. (1) with $N = 3$, where the external potential is

$(U_1,U_2,U_3) = (\Delta,0,-\Delta)$. In the absence of Δ, the Hamiltonian can be block-diagonalized into a monolayer-like band and a bilayer-like band.[30] In finite Δ, these subblocks are hybridized, and it is then useful to arrange the basis as

$$\begin{aligned}&\{(|A_1\rangle - |A_3\rangle)/\sqrt{2},\ |B_2\rangle,\quad (|B_1\rangle + |B_3\rangle)/\sqrt{2},\\ &(|B_1\rangle - |B_3\rangle)/\sqrt{2},\ |A_2\rangle,\quad (|A_1\rangle + |A_3\rangle)/\sqrt{2}\},\end{aligned} \tag{2}$$

where the monolayer-like band corresponds to first and fourth bases, and the bilayer-like band corresponds to second, third, fifth, and sixth. We categorize the first three bases in Eq. (2) as group $\circ$ and the last three as group $\bullet$. The Hamiltonian is written in this basis as

$$\mathcal{H} = \begin{pmatrix} H_\circ & D_- \\ D_+ & H_\bullet \end{pmatrix}, \tag{3}$$

$$D_+ = \begin{pmatrix} v\pi & 0 & \Delta \\ 0 & v\pi^\dagger & \sqrt{2}\gamma_1 \\ \Delta & \sqrt{2}v_3\pi & v\pi^\dagger \end{pmatrix}, \quad D_- = (D_+)^\dagger, \tag{4}$$

$$H_\circ = \begin{pmatrix} -\gamma_2/2 & 0 & 0 \\ 0 & 0 & -\sqrt{2}v_4\pi \\ 0 & -\sqrt{2}v_4\pi^\dagger & \gamma_5/2 + \Delta' \end{pmatrix}, \tag{5}$$

$$H_\bullet = \begin{pmatrix} -\gamma_5/2 + \Delta' & 0 & 0 \\ 0 & \Delta' & -\sqrt{2}v_4\pi \\ 0 & -\sqrt{2}v_4\pi^\dagger & \gamma_2/2 \end{pmatrix}. \tag{6}$$

If we keep only relevant band parameters $\gamma_0,\gamma_1,\gamma_3$ and the potential Δ, and neglect the remaining parameters, the Hamiltonian Eq. (3) possesses chiral symmetry (sublattice symmetry) in that the diagonal matrix blocks $H_\circ$ and $H_\bullet$ all vanish, leaving the off-diagonal blocks $D_\pm$ which connect the bases of $\circ$ to the bases of $\bullet$. The reason for this can be understood in terms of reflection symmetry as follows: In the group $\circ$ ($\bullet$), the bases associated with A and B sublattices have odd and even (even and odd) parity, respectively, with respect to the reflection in the middle layer. The Hamiltonian without Δ, i.e., the first term in Eq. (1), has even parity in the reflection, and has matrix elements only between A and B sublattices when only γ_0, γ_1, and γ_3 are kept. After the unitary transformation, it does not give any matrix elements in $H_\circ$ or $H_\bullet$ because in each group ($\circ$ or $\bullet$), a base associated with A and one associated with B always have different parity from the definition. On the other hand, the potential term, i.e., the second term in Eq. (1), is odd in the reflection and matrix elements only connect the same sublattice. It gives no matrix elements in $H_\circ$ or $H_\bullet$ either, because in each group, bases associated with the same sublattice always have the same parity.

The energy spectrum of this simplified Hamiltonian contains a single center Dirac cone and six off-center Dirac cones at zero energy, as depicted in Fig. 1(a). The robustness of the gapless spectrum is protected by the chiral symmetry. The extra terms with γ_2, γ_5, v_4, and Δ' in the diagonal blocks break the chiral symmetry and open small energy gaps at these Dirac cones, as shown in Fig. 1(b).

The positions of the Dirac points in the chiral Hamiltonian without $H_\circ$ and $H_\bullet$ can be found by solving $\det D_+ = 0$ with $\pi = \xi p_x + ip_y = pe^{i\theta}$. We obtain a Dirac point at $p = 0$, and six off-center Dirac points at

$$\begin{aligned} &p = p_+; \quad \theta = 0, \frac{2\pi}{3}, \frac{4\pi}{3}, \\ &p = p_-; \quad \theta = \frac{\pi}{3}, \pi, \frac{5\pi}{3}, \\ &p_\pm = \frac{\pm\gamma_1 v_3 + \sqrt{\Delta^2 v^2 + \gamma_1^2 v_3^2}}{v^2}. \end{aligned} \tag{7}$$

At each Dirac point, the degenerate zero-energy bases $\psi_\circ$ and $\psi_\bullet$ are derived from the equation $D_+|\psi_\circ\rangle = 0$ and $D_-|\psi_\bullet\rangle = 0$, and the effective Dirac Hamiltonian is given by

$$H_{\text{eff}} = \begin{pmatrix} 0 & \langle\psi_\circ|D_-|\psi_\bullet\rangle \\ \langle\psi_\bullet|D_+|\psi_\circ\rangle & 0 \end{pmatrix}, \tag{8}$$

keeping the lowest order in the momentum shift from the Dirac point. By rotating the (x,y) coordinates and the spinor space by angle θ at the same time, this is transformed to

$$H_{\text{eff}} = v_x\tilde{\pi}_x\sigma_x + v_y\tilde{\pi}_y\sigma_y, \tag{9}$$

where σ_x and σ_y are Pauli matrices and $(\tilde{\pi}_x,\tilde{\pi}_y)$ is the momentum measured from each Dirac point. We find for the Dirac point at $p = 0$ (no need for rotation)

$$\begin{aligned} &\psi_\circ = (0,1,0), \\ &\psi_\bullet = (-\sqrt{2}\gamma_1,\Delta,0)/\sqrt{\Delta^2 + 2\gamma_1^2}, \end{aligned} \tag{10}$$

and

$$v_x = \xi\frac{\Delta v}{\sqrt{\Delta^2 + 2\gamma_1^2}}, \quad v_y = -\frac{\Delta v}{\sqrt{\Delta^2 + 2\gamma_1^2}} \tag{11}$$

with the valley index $\xi = \pm$. For the off-center Dirac points at $p = p_\pm$,

$$\begin{aligned} &\psi_\circ = (-\Delta e^{i\theta}, \mp\sqrt{2}\gamma_1, vp_\pm e^{2i\theta})/C_1, \\ &\psi_\bullet = (-\Delta, \mp\sqrt{2}v_3 p_\pm, vp_\pm e^{-i\theta})/C_2, \\ &C_1 = \sqrt{\Delta^2 + 2\gamma_1^2 + v^2 p_\pm^2}, \quad C_2 = \sqrt{\Delta^2 + \left(2v_3^2 + v^2\right)p_\pm^2}, \end{aligned} \tag{12}$$

and the velocities after rotation of (x,y) by θ become

$$\begin{aligned} v_x &= 2\xi v(\pm\Delta^2 + \gamma_1 v_3 p_\pm)/(C_1 C_2), \\ v_y &= -6\gamma_1 v_3 v p_\pm/(C_1 C_2), \end{aligned} \tag{13}$$

where v_x and v_y correspond to the radial and azimuthal directions, respectively, with respect to $p = 0$. v_x and v_y of each Dirac point are plotted in Fig. 3(d). The velocities are mainly enhanced by applying Δ, while v_y for p_+ decreases only slowly. This indicates that the conductivity, which is roughly proportional to the square of the band velocity,[5] is enhanced by Δ, as is consistent with the previous transport measurement[17] and the theoretical estimation.[30]

The chirality for each Dirac cone can be defined by $\nu_c \equiv \text{sgn}(v_x v_y)$, and this coincides with the Berry phase in units of π around the Dirac point. We find $\nu_c = -\xi$ for $p = 0$ and $\nu_c = \mp\xi$ for $p = p_\pm$, so that the summation of chirality over seven Dirac points in the valley K_ξ is $-\xi$. Since the chirality is a topologically protected number as long as the chiral symmetry is present, nonzero total chirality indicates that the conduction band and the valence band inevitably touch at some points in any value of Δ.

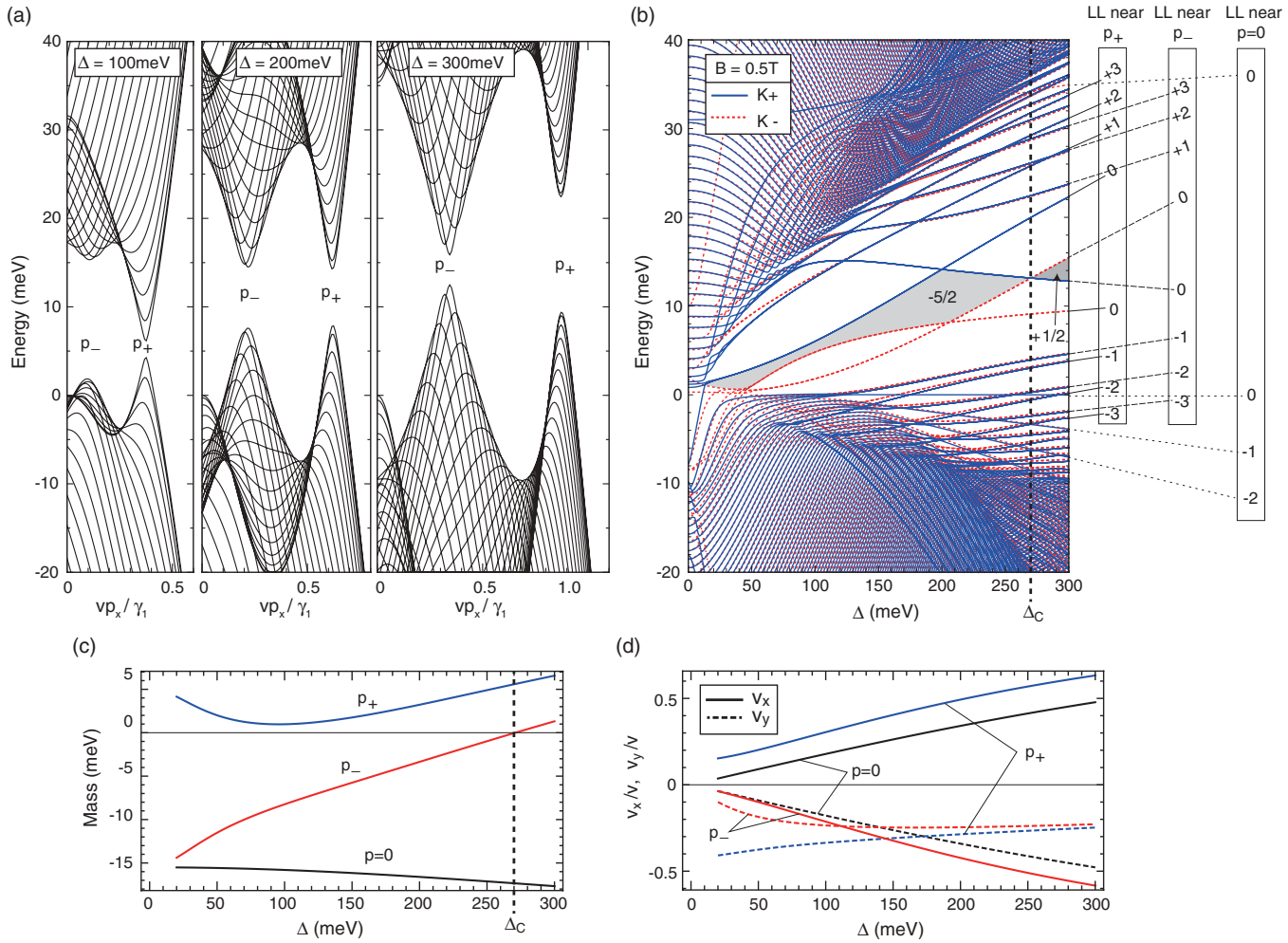

FIG. 3. (Color online) (a) Band structure of gated ABA trilayer with various potential asymmetry Δ. (b) Gate bias dependence of Landau-level energy in $B = 0.5$ T. Landau levels in K_+ and K_- valleys are plotted as solid (blue) and dashed (red) lines, respectively. Shaded area represents the charge neutral region, where the number indicates the single-valley Hall conductivity $\sigma_{xy}^{K\xi}$ in units of $\xi e^2/h$. (c) Effective mass m and (d) band velocities v_x, v_y for the effective Dirac cones at $p = 0, p_+, p_-$, plotted against Δ.

Now we consider all the band parameters in Eq. (3) to argue the energy gaps at the Dirac points. The effective Hamiltonian of each gate-induced Dirac cone is modified to

$$H_{\text{eff}} = v_x\tilde{\pi}_x\sigma_x + v_y\tilde{\pi}_y\sigma_y + m\sigma_z + \epsilon_0 I, \tag{14}$$

where the mass m and the energy shift ϵ_0 are given by

$$m = [\langle\psi_\circ|H_\circ|\psi_\circ\rangle - \langle\psi_\bullet|H_\bullet|\psi_\bullet\rangle]/2, \tag{15}$$

$$\epsilon_0 = [\langle\psi_\circ|H_\circ|\psi_\circ\rangle + \langle\psi_\bullet|H_\bullet|\psi_\bullet\rangle]/2. \tag{16}$$

The width of the energy gap is $2m$. Note that the approximation using the gapped Dirac Hamiltonian above is valid when the mass gap is smaller than the energy region of the gate-induced Dirac cone below the Lifshitz transition point. In Fig. 3(c), we show the evaluated mass m for the seven Dirac points. We see that the mass for $p = p_-$ changes from negative to positive when Δ exceeds the critical value,

$$\Delta_c \approx 270 \text{ meV}, \tag{17}$$

at which the energy gap closes.

When the Fermi energy lies in the gap in massive Dirac Hamiltonian Eq. (14), the Hall conductivity takes nonzero value $\sigma_{xy} = [e^2/(2h)]\text{sgn}(v_x v_y m)$ even in zero magnetic field.[50,51] Considering the chirality and mass for each Dirac point in Table I, the total Hall conductivity summed over the Dirac points at single-valley K_ξ becomes

$$\sigma_{xy}^{K_\xi} = \frac{e^2}{h} \times \begin{cases} -\frac{5}{2}\xi & (\Delta < \Delta_c), \\ +\frac{1}{2}\xi & (\Delta > \Delta_c). \end{cases} \tag{18}$$

TABLE I. Sign of chirality, mass, and in-gap Hall conductivity for gate-induced Dirac cones at the K_ξ valley.

p	0 ($\times 1$)	p_+ ($\times 3$)	p_- ($\times 3$)
$\text{sgn}(v_x v_y)$	$-\xi$	$-\xi$	$+\xi$
$\text{sgn}(m)$	-1	$+1$	$\begin{cases} -1(\Delta < \Delta_c) \\ +1(\Delta > \Delta_c) \end{cases}$
$\text{sgn}(v_x v_y m)$	$+\xi$	$-\xi$	$\begin{cases} -\xi(\Delta < \Delta_c) \\ +\xi(\Delta > \Delta_c) \end{cases}$

We have a topological change at gap closing point, $\Delta = \Delta_c$. The Hall conductivity has opposite signs between two valleys $K_\pm$ due to the time-reversal symmetry, so that the net Hall conductivity is always zero. Nevertheless, the single-valley Hall conductivity is directly related to the number of chiral edge modes appearing in the zigzag edge, as we will see in Sec. III C.

B. Landau-level structure

The Landau levels in the presence of a uniform magnetic field $\boldsymbol{B} = (0,0,B)$ can be calculated by the Hamiltonian with $\pi = (\sqrt{2}\hbar/\ell)a^\dagger$ and $(\sqrt{2}\hbar/\ell)a$ for K_+ and K_-, respectively. Here $a^\dagger$ and a are raising and lowering operators, respectively, which operate on the Landau-level wave function ϕ_n as $a\phi_n = \sqrt{n}\phi_{n-1}, a^\dagger\phi_n = \sqrt{n+1}\phi_{n+1}$, and $\ell = \sqrt{\hbar/(eB)}$ is the magnetic length. The Landau-level spectrum at $B = 0.5$ T is plotted as a function of potential asymmetry Δ in Fig. 3(b). Landau levels in K_+ and K_- valleys are plotted as solid (blue) and dashed (red) lines, respectively. There we can see two distinct regions, a region around zero energy where the Landau-level spacing is wide due to Dirac Landau levels, and a region above the Lifshitz transition where the Landau levels are densely spaced due to the large density of states. In increasing Δ, the gate-induced Dirac pockets accommodate more and more Landau levels as the energy region within the Dirac pockets expands.

The low-energy Landau levels inside the gate-induced Dirac pockets can be approximately described by the massive Dirac Hamiltonian, Eq. (14). There the Landau-level spectrum is explicitly written as

$$\begin{aligned} E_0 &= \epsilon_0 - \mathrm{sgn}(v_x v_y)\, m, \\ E_{\pm n} &= \epsilon_0 \pm \sqrt{\Delta_B^2 n + m^2}, \quad (n > 0), \end{aligned} \tag{19}$$

where

$$\Delta_B = \sqrt{2|v_x v_y|\hbar e B}. \tag{20}$$

We note that the Landau level of $n = 0$ is sensitive to the chirality and the sign of the mass: it appears at the top of the valence band and the bottom of the conduction band when $\mathrm{sgn}(v_x v_y m) > 0$ and < 0, respectively. The two cases correspond to the midgap values of the Hall conductivity, $\sigma_{xy} = e^2/(2h)$ and $-e^2/(2h)$, respectively. Also, since the chirality $\mathrm{sgn}(v_x v_y)$ is opposite between K_+ and K_- valleys, the $n = 0$ Landau-level splits in valleys while all others are valley-degenerate. Besides, we have additional triplefold degeneracies for each of p_+ and p_-.

In Fig. 3(b), we actually see that the $n = 0$ level is nondegenerate in valleys, appearing at either of the band edges of each massive Dirac band. At $\Delta = \Delta_c$, we observe that one pair of $n = 0$ levels from $K_\pm$ valleys cross each other at the charge neutral point, in accordance with the topological change of $\sigma_{xy}^{K_\xi}$ from $(-5/2)\xi e^2/h$ to $(+1/2)\xi e^2/h$. The $n > 0$ levels are almost valley-degenerate, while a tiny splitting is due to the deviation from the massive Dirac Hamiltonian Eq. (14).

When we drop the band parameters other than γ_0, γ_1, and γ_3, the Hamiltonian becomes chiral symmetric and the zeroth Landau level E_0 of each Dirac cone comes exactly to zero energy as a chiral zero mode, of which the wave function has amplitude only on $\circ$ and $\bullet$ for $v_c = \mp\xi$, respectively. The index theorem then states that the difference between the number of the zero modes belonging to $\circ$ (n_+) and those to $\bullet$ (n_-) is defined as the chiral index, which coincides with the gauge flux penetrating the system. The chiral index in the present case is shown to be $n_+ - n_- = \xi\Phi$, where $\Phi = eBS/h$ is the magnetic flux penetrating the system area S. This is, in units of Φ, coherent with a summation of $-v_c$ in each single valley. As in the conventional Dirac Hamiltonian,[52–54] the chiral index can be related to the geometric curvature of the gauge field, and the above relation between the chiral index and total magnetic flux stands in nonuniform magnetic field as well. A detailed argument is presented in Appendix A.

C. Edge modes

Nontrivial Hall conductivity in a single valley indicates the existence of chiral edge modes localized at the interface, as long as the valley mixing is not present. There the number of emergent edge modes is directly related to the Hall conductivity, so that chiral edge modes as many as the number of $\sigma_{xy}^{K_\pm}$ should counterflow in opposite directions between K_+ and K_-, as is analogous to the spin Hall insulator.[42] Here we numerically examined the edge modes in the asymmetric ABA-trilayer graphene with zigzag interfaces, in which the valley mixing is absent. We consider a semi-infinite system with a zigzag boundary along the x direction as shown in Fig. 4(a), where p_x is a good quantum number. The energy of edge modes in the bulk gap can be obtained by searching for the evanescent modes satisfying a boundary condition at the interface. The method is detailed in Appendix B.

First we consider the chiral symmetric case neglecting $\gamma_2, \gamma_5, v_4, \Delta'$. Figure 4 illustrates the energy spectrum near the K_+ point at $\Delta = 200$ meV, where we see that zero-energy edge modes appear between some of the gate-induced Dirac points. The number of zero-energy edge modes is closely related to the chirality of each Dirac cone.[55–58] When we regard a two-dimensional periodic system on the x-y plane as a one-dimensional system with fixed p_x as a parameter, we can define a winding number $\gamma(p_x)$ by integrating the Berry phase change all the way along p_y on the Brillouin zone at the fixed p_x. When we set the boundary perpendicular to the y axis (i.e., p_x is still a good quantum number), the number of zero-energy edge modes appearing at the boundary coincides with $\gamma(p_x)$ except a constant.[55] In the present system, this bulk-edge relationship can be clearly seen in Fig. 4.

Other hopping terms breaking the chiral symmetry give rise to mass of the Dirac points, and relative signs between these masses determine the connection of the chiral edge modes between different Dirac points. In Fig. 5(a), we plot the band structure near K_+ including full band parameters at $\Delta = 200$ meV. We see that the left and right edge modes stick to either the top or bottom gapped Dirac cone depending on the sign of the mass. At the charge neutral point, we have three sets of chiral edge channels crossing the Fermi energy, which all circulate in a clockwise direction when viewed from the $+z$ direction. We also observe two edge states extending out of the plot and leading to the other valley K_-. In K_-, we have the exact same spectrum with p_x inverted to $-p_x$.

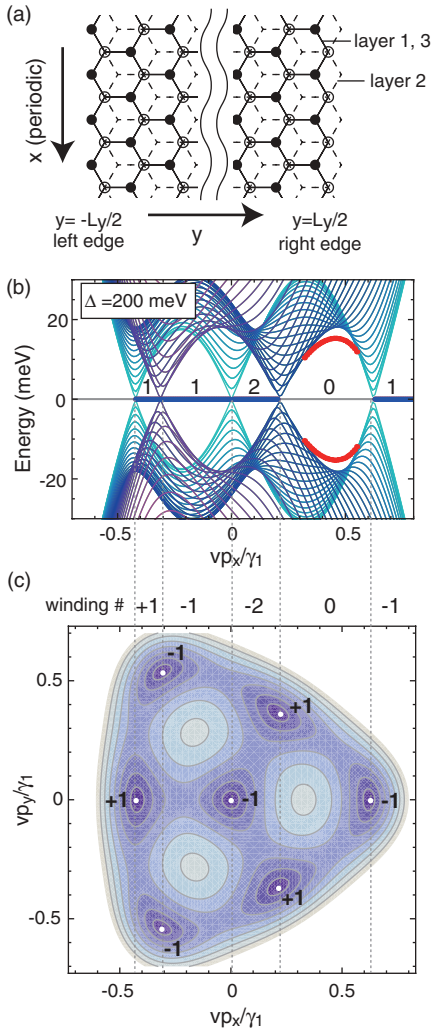

FIG. 4. (Color online) (a) Atomic structure of a zigzag ribbon of ABA-trilayer graphene. (b) Band structure around the K_+ valley of a zigzag ribbon of ABA-trilayer graphene only including γ_0, γ_1, and γ_3, with the asymmetric potential $\Delta = 200$ meV. Bulk, left-edge, and right-edge states are plotted with solid lines, red dots, and blue dots, respectively. Numbers indicate the degeneracies of the edge-state bands for a single side (the same for the left and the right edges). (c) Contour plot of the bulk band structure with white dots and labels denoting the position and the chirality of gate-induced Dirac points, respectively. One-dimensional winding number $\gamma(k_x)$ is indicated between dotted lines penetrating the Dirac points.

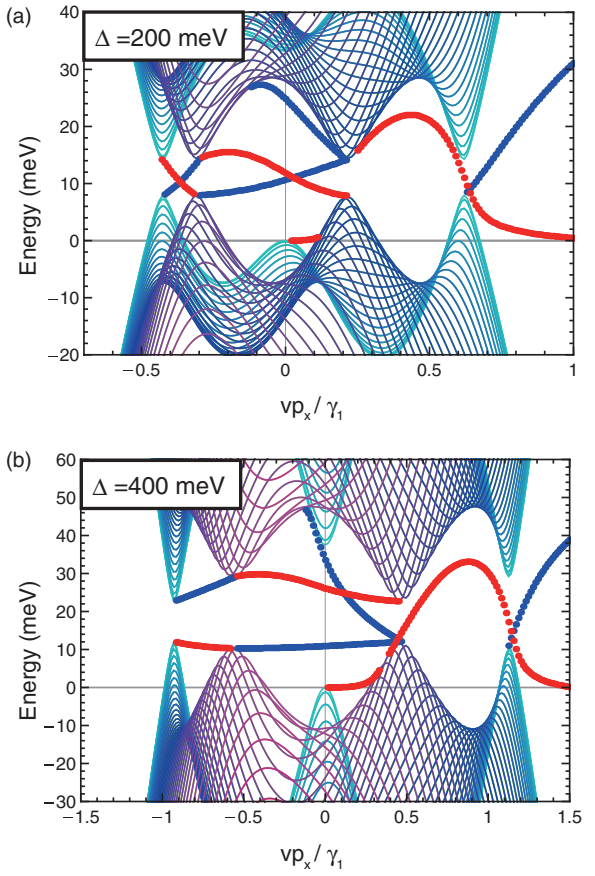

FIG. 5. (Color online) Band structure around the K_+ valley of zigzag ribbon of ABA-trilayer graphene with the parameters fully included, in the asymmetric potential (a) $\Delta = 200$ meV and (b) $\Delta = 400$ meV. Bulk, left-edge, and right-edge states are plotted with solid lines, red dots, and blue dots, respectively.

The correspondence with the single-valley Hall conductivity can be understood using a similar argument to that for the integer quantum Hall effect.[59] Let us consider a cylindrical system which is closed in x with circumference L_x while finite in the axial direction y with $-L_y/2 < y < L_y/2$ bound by the zigzag edges. When we adiabatically turn on a magnetic flux quantum h/e penetrating into the cylinder (inducing an electric field along the $-x$ direction), every state at p_x is shifted to $p_x + 2\pi\hbar/L_x$. The single-valley Hall conductivity of K_+ then coincides with the total move of K_+ electrons in the $-y$ direction through this adiabatic process. At the Fermi energy, an electron moves from the left edge to the right for each of three pairs of counterpropagating channels, contributing to $\sigma_{xy}^{K_+} = -3e^2/h$. A charge transfer also occurs below the Fermi energy, where a bulk state ($\langle y\rangle = 0$) is pumped to an edge state ($\langle y\rangle = -L_y/2$) in the left-edge channel going out of the valley. This yields a contribution to $\sigma_{xy}^{K_+} = (+1/2)e^2/h$, which adds up to $\sigma_{xy}^{K_+} = (-5/2)e^2/h$ all together.

Figure 5(b) plots the band structure at larger bias, $\Delta = 400$ meV after the topological transition at Δ_c. We find that the connection of the edge modes changes at $p = p_-$, leaving only one clockwise and one anticlockwise chiral edge mode crossing at the Fermi energy. The Hall conductivity from those two exactly cancel out, while we have the same contribution from the edge channel below the Fermi energy, giving the total Hall conductivity $\sigma_{xy}^{K_+} = (+1/2)e^2/h$. This again coincides with bulk valley Hall conductivity estimated from the mass and chirality. Conversely, the single-valley Hall conductivity gives the number of counteredge modes crossing at the Fermi energy, when we appropriately exclude the half-integer contribution from the edge modes connecting $K_\pm$.

IV. FOUR-LAYER GRAPHENE

Unlike trilayer, a four-layer graphene with interlayer asymmetry does not possess chiral symmetry even in the approximate model, and the band gap is always open at zero

energy. The effective low-energy Hamiltonian can be obtained by excluding the high-energy bonding states at $|\varepsilon| \sim O(\gamma_1)$ as $H_{\rm eff} = H_{11} - H_{12}H_{22}^{-1}H_{21}$,[21] where H_{11} and H_{22} represent diagonal blocks of the original Hamiltonian for low-energy bases spanned by $(A1, B2, A3, B4)$ and for high-energy bases by $(B1, A2, B3, A4)$, respectively, and H_{12} and H_{21} are off-diagonal blocks connecting them. This is explicitly written in basis $(A1, B2, A3, B4)$ as

$$H_{\rm eff} = \frac{v^2}{\gamma_1}\begin{pmatrix} 0 & -(\pi^\dagger)^2 & 0 & (\pi^\dagger)^2 \\ -\pi^2 & 0 & 0 & 0 \\ 0 & 0 & 0 & -(\pi^\dagger)^2 \\ \pi^2 & 0 & -\pi^2 & 0 \end{pmatrix} + v_3\begin{pmatrix} 0 & \pi & & \\ \pi^\dagger & 0 & \pi^\dagger & \\ & \pi & 0 & \pi \\ & & \pi^\dagger & 0 \end{pmatrix} + \Delta\begin{pmatrix} \frac{3}{2} & & & \\ & \frac{1}{2} & & \\ & & -\frac{1}{2} & \\ & & & -\frac{3}{2} \end{pmatrix}, \tag{21}$$

where we neglected the band parameters other than γ_0, γ_1, and γ_3. The approximation is valid only when $vp, \Delta \ll \gamma_1$.

If we even neglect the v_3 term, the low-energy energy band is rotationally symmetric around $K\pm$ points and its dispersion relation is given by

$$\epsilon(p) = \pm\tfrac{1}{2}\sqrt{6\tilde{\epsilon}^2 + 5\Delta^2 - 2\sqrt{5\tilde{\epsilon}^4 + 20\tilde{\epsilon}^2\Delta^2 + 4\Delta^4}} \tag{22}$$

with $\tilde{\epsilon} = v^2p^2/\gamma_1$. The band gap appears between $\varepsilon = \pm(\Delta/2)(-7 + 16/\sqrt{5})^{1/2}$, corresponding to an off-center momentum $p_0 = (-2 + 6/\sqrt{5})^{1/4}\sqrt{\gamma_1\Delta}/v$.

When we resume the v_3 term and other parameters, six off-center pockets emerge at momentum p_+ and p_- near p_0, each of which are arranged in 120° symmetry as illustrated in Figs. 6 and 7(a). The preexisting gap never closes during this process. The pockets at $p = p_+$ are much deeper than those at $p = p_-$, and the energy depth is about 15 meV at $\Delta = 100$ meV. Figure 7(b) describes an evolution of Landau-level energies with increasing Δ, where we observe the triply degenerate Landau levels of p_+ pockets with wide energy spacing, similarly to trilayer graphene.

We can expand the Hamiltonian with respect to the center of each Dirac pocket, and we obtain the effective 2×2 Hamiltonian in the massive Dirac form of Eq. (14). The masses and the velocities are shown in Figs. 7(c) and 7(d), respectively, where we set the basis so that the chirality becomes +1 (i.e., $v_x v_y$ positive). The masses at p_+ and p_- are opposite in sign, so that the contributions to the Hall conductivity of Dirac cones cancel out in summation over a single valley. Therefore, the single-valley system is a trivial insulator with zero Hall conductivity in contrast to trilayer graphene. Accordingly, we observe no Landau-level crossing at a charge neutral point in Fig. 7(b), and if we look at the edge states in Fig. 7(e), there are no edge channel crossing in the bulk gap nor the counterpropagating flows of valley pseudospin.

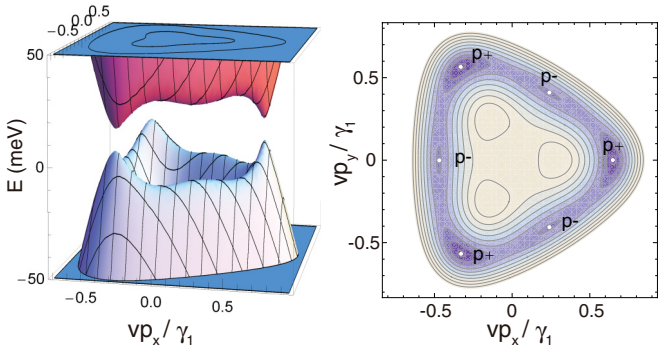

FIG. 6. (Color online) Band structures of ABA-stacked four-layer graphene with the interlayer asymmetric potential $\Delta = 100$ meV, depicted in a 3D plot (left panel) and contour plot (right).

V. GENERAL ODD-LAYER GRAPHENES

The approximate chiral symmetry in the presence of the external electric field argued in a trilayer actually holds in any odd-layer Bernal multilayer graphenes. As we see in the following, if we only consider $\gamma_0, \gamma_1, \gamma_3, \Delta$ terms, the Hamiltonian of odd-layer graphene is chiral symmetric with a nonzero chiral index in the presence of magnetic field, which means that the band is gapless in the limit of zero magnetic field.

The Hamiltonian for Bernal stacked N-layer graphene is decomposed into block diagonal form with effective monolayer and bilayer blocks with a unitary transformation.[28,29,31,32] Let us define

$$\begin{aligned} f_m(j) &= c_m\sqrt{\frac{2}{N+1}}[1 - (-1)^j]\sin\kappa_m j, \\ g_m(j) &= c_m\sqrt{\frac{2}{N+1}}[1 + (-1)^j]\sin\kappa_m j, \end{aligned} \tag{23}$$

where

$$\begin{aligned} \kappa_m &= \frac{\pi}{2} - \frac{m\pi}{2(N+1)}, \\ c_m &= \begin{cases} 1/2 & (m = 0), \\ 1/\sqrt{2} & (m \neq 0), \end{cases} \end{aligned} \tag{24}$$

$j = 1, 2, \ldots, N$ is the layer index, and m is the block index given as

$$m = \begin{cases} 1,3,5,\ldots,N-1, & \text{where } N \text{ is even}, \\ 0,2,4,\ldots,N, & \text{where } N \text{ is odd}. \end{cases}$$

Then we take a basis

$$\begin{aligned} \left|\phi_m^{(X,\text{odd})}\right\rangle &= \sum_{j=1}^{N} f_m(j)|X_j\rangle, \\ \left|\phi_m^{(X,\text{even})}\right\rangle &= \sum_{j=1}^{N} g_m(j)|X_j\rangle, \end{aligned} \tag{25}$$

where $X = A$ or B. A superscript (X,odd) $[(X,\text{even})]$ indicates that the wave function is nonzero only on the sublattice X on the layer $j =$ odd (even).

With the above basis set, the Hamiltonian with $\Delta = 0$ is block diagonalized with m. A block labeled by m spanned by $\{|\phi_m^{(A,\text{odd})}\rangle, |\phi_m^{(B,\text{odd})}\rangle, |\phi_m^{(A,\text{even})}\rangle, |\phi_m^{(B,\text{even})}\rangle\}$ is dictated as

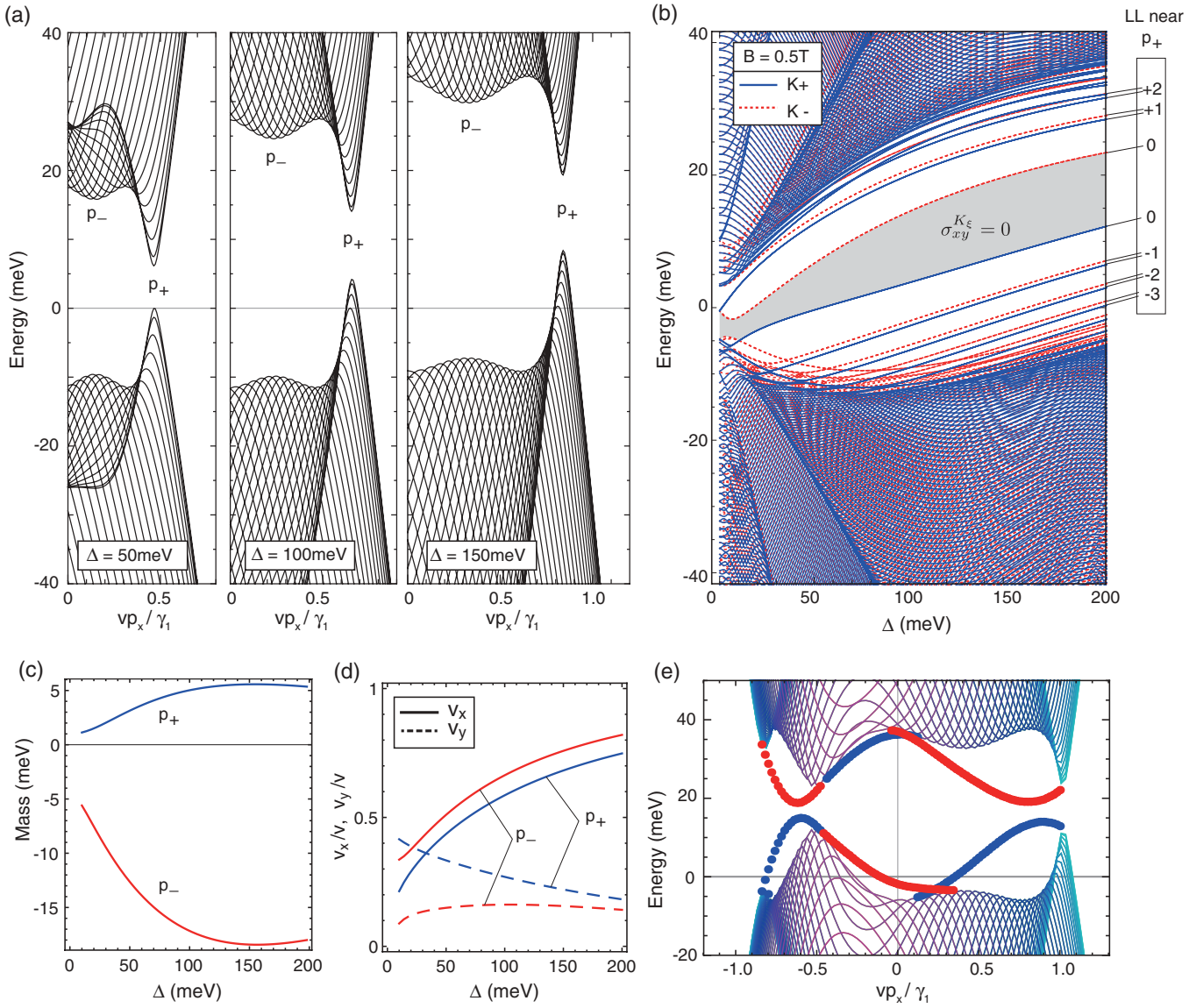

FIG. 7. (Color online) Plots similar to Fig. 3 for ABA four-layer graphene. (a) Band structure with various potential asymmetry Δ. (b) Gate bias dependence of Landau-level energy in $B = 0.5$ T. Shaded area represents the charge neutral region. (c) Effective mass m and (d) band velocities v_x, v_y for the effective Dirac cones at p_+, p_-, plotted against Δ. (e) Band structure similar to Fig. 5 for zigzag ribbon of ABA four layer with $\Delta = 200$ meV.

$H(\lambda_m)$ with $\lambda_m = 2\cos\kappa_m$ and

$$H(\lambda) = \begin{pmatrix} 0 & v\pi^\dagger & 0 & \lambda v_3\pi \\ v\pi & 0 & \lambda\gamma_1 & 0 \\ 0 & \lambda\gamma_1 & 0 & v\pi^\dagger \\ \lambda v_3\pi^\dagger & 0 & v\pi & 0 \end{pmatrix}, \tag{26}$$

where we only left the terms with $\gamma_0, \gamma_1, \gamma_3$, For the case of $m = 0$, only two bases $|\phi_m^{(A,\mathrm{odd})}\rangle, |\phi_m^{(B,\mathrm{odd})}\rangle$ survive due to $g_0(j) = 0$, and the corresponding block Hamiltonian is the first 2 by 2 component of Eq. (26).

Now let us consider an odd-layer graphene with the interlayer potential asymmetry $U(\Delta)$, i.e., the second term of the Hamiltonian, Eq. (1). When N is odd, we can easily show that the basis function belonging to the block m is either symmetric or antisymmetric with respect to reflection in the central layer $j = (N+1)/2$, and the parity is given by $(-1)^{(N-m-1)/2}$.[32] If we write down $U(\Delta)$ in this basis, the matrix element $\langle\phi_{m'}^{(X',p')}|U|\phi_m^{(X,p)}\rangle$ ($p, p' =$ even or odd) becomes nonzero only when $m' = m + 4l + 2$ (l is an integer), $X = X'$, and $p = p'$, because U is an odd function in the reflection and is also diagonal in the original site representation.

Therefore, if we separate the basis functions into two groups $\circ, \bullet$ as

$$\left(|\phi_m^{(A,\mathrm{odd})}\rangle, |\phi_m^{(B,\mathrm{odd})}\rangle, |\phi_m^{(A,\mathrm{even})}\rangle, |\phi_m^{(B,\mathrm{even})}\rangle\right) \in \begin{cases} (\circ, \bullet, \circ, \bullet) & (m = 4l), \\ (\bullet, \circ, \bullet, \circ) & (m = 4l+2), \end{cases} \tag{27}$$

then the Hamiltonian including only $\gamma_0, \gamma_1, \gamma_3, \Delta$ has matrix elements only between $\circ$ and $\bullet$, and thus is chiral symmetric. Note that the chiral symmetry does not hold for even-layer graphenes since the basis function labeled by m cannot be

categorized to either even or odd parity, and the interlayer potential term gives rise to matrix elements connecting blocks m and $m+4l$.

In the presence of a magnetic field, the chiral index, i.e., the difference between the number of the zero modes belonging to $\circ$ (n_+) and those to $\bullet$ (n_-), can be easily obtained by considering the Landau-level spectrum with γ_1, v_3, and Δ all switched off, since the chiral index never changes in such a continuous transformation. The bilayer-like Hamiltonian block, Eq. (26), then consists of two monolayer-type 2×2 diagonal blocks, giving two zero-energy Landau levels localized at the second and fourth (first and third) elements in the valley $\xi = +(-)$. Considering the base grouping in Eq. (27), the difference in zero-energy states in block m is found to be $n_+ - n_- = \mp 2\xi\Phi$ for $m = 4l$ and $m = 4l+2$, respectively, where $\Phi = eBS/h$ is the magnetic flux penetrating the system. The monolayer-type block $m = 0$ lacks the third and fourth elements, giving $n_+ - n_- = -\xi\Phi$. As a result, the total chiral index in odd-layer graphene for valley K_ξ is finally given by

$$n_+ - n_- = (-1+2-2+2\ldots)\xi\Phi = \begin{cases} -\xi\Phi, & N = 4l+1, \\ +\xi\Phi, & N = 4l+3. \end{cases} \tag{28}$$

This states that at least one Landau level remains at zero energy, and thus in zero magnetic field the conduction and valence band touch at one k point at least. The sum of Berry phases in a single valley coincides with $-\pi$ times the chiral index in units of Φ, that is, $\pm\xi\pi$ for $N = 4l+1$ and $4l+3$, respectively. When the Dirac cones are gapped by including the additional band parameters, the Hall conductivity per single valley must be nonzero, because the number of Dirac cones per valley must be odd to achieve total Berry phase $\pm\pi$.

This result might seem to contradict the well-known fact that the Berry phase is $N\pi$ in N-layer graphene at $\Delta = 0$. As argued, the Hamiltonian with $\Delta = 0$ is block-diagonalized into independent monolayer-like and bilayer-like subsystems. In each block, there is an ambiguity in the choice of bases for $\circ$ or $\bullet$, and the Berry phase of the block actually changes its sign when $\circ$ and $\bullet$ are interchanged. If we simply assign all A and B sublattices to $\circ$ and $\bullet$, respectively, we obtain $n_+ - n_- = (-1-2-2-2\ldots)\xi\Phi = -\xi N\Phi$ instead of Eq. (28). In the presence of nonzero Δ, on the other hand, the subsystems are mixed with each other and then the grouping of Eq. (27) is the only possible way to make the Hamiltonian chiral symmetric.

VI. CONCLUSION

In Bernal multilayer graphene, more than three layers, an interplay of the gate electric field and the trigonal warping effect, give rise to emergent Dirac cones in the low-energy bands, whose band velocity and Lifshitz transition energy are tunable by the gate voltage. In trilayer graphene, in particular, the low-energy effective theory shows that the valley Hall state is realized at the charge neutral point, where single-valley Hall conductivity is quantized at a nonzero half-integer. We have investigated the edge states at the zigzag interface and demonstrated that the number of edge modes is closely related to the bulk single-valley Hall conductivity. In four-layer graphene, gate-induced Dirac cones also appear, though the system is a trivial insulator with zero-valley Hall conductivity. The nontrivial valley Hall state is generally found in odd-layer graphenes, where the approximate chiral symmetry is responsible for the emergence of nonzero-valley Hall conductivity.

The gate-induced Dirac cones should be experimentally accessible directly by observing Landau levels with wide energy spacing.[60–62] Also, the single-valley Hall conductivity argued here is expected to be observable in the transport through the edge modes at a zigzag interface, while a valley mixing caused by a concentration of atomic-scale scatterers or the presence of an armchair edge would dilute the effect. There the conductance is related to the number of edge channels, and the topological transition at Δ_c should be observed as a change in the conductance. Since the helical edge modes appearing in the gated multilayer graphene carry valley pseudospins, modulation of edge modes through the gate voltage could be a way to electrically control the valley polarized transport.

ACKNOWLEDGMENTS

We would like to acknowledge helpful discussions with Akira Furusaki. This work was supported by Grants-in-Aid for Scientific Research, No. 24840047 (T.M.) and No. 24740193 (M.K.), from JSPS.

APPENDIX A: INDEX THEOREM FOR ODD-LAYER GRAPHENES

Here we show that the chiral index of general odd-layer graphenes can be written in terms of the total gauge flux penetrating the system, in a similar way to the argument for the usual Dirac Hamiltonian.[52–54] The chiral symmetric Hamiltonian of odd-layer graphene with interlayer asymmetric potential is written as

$$H = \begin{pmatrix} 0 & D_- \\ D_+ & 0 \end{pmatrix}, \tag{A1}$$

where $D_+ = (D_-)^\dagger$ is an $N\times N$ matrix. The chiral symmetry is then expressed by $\Gamma H + H\Gamma = 0$ with the chiral operator Γ,

$$\Gamma = \begin{pmatrix} \mathbb{1}_N & 0 \\ 0 & -\mathbb{1}_N \end{pmatrix},$$

where $\mathbb{1}_N$ is an $N\times N$ unit matrix. We can take zero modes of H as an eigenvector $\psi_\pm$ of Γ with eigenvalue ± 1, respectively. If we write the number of chiral zero modes $\psi_\pm$ as $n_\pm$, the chiral index ν is defined as

$$\nu = n_+ - n_- = \mathrm{Tr}\Gamma f(H^2/M^2),$$

where f is a regularization function, which is a smooth and monotonically decreasing function with $f(0) = 1$ and $f(\infty) = 0$, and M is an ultraviolet cutoff. The action of f to the matrix is defined through its action onto the eigenvalues, as seen if we take $f(z) = e^{-z}$.

If we take plane waves $\exp(i\boldsymbol{k}\cdot\boldsymbol{x})$ as a basis for the spatial direction, we have

$$\begin{aligned}\nu &= \mathrm{Tr}\Gamma f(H^2/M^2)\\ &= \mathrm{Tr}[f(D_-D_+/M^2) - f(D_+D_-/M^2)]\\ &= \int d^2x \int \frac{d^2k}{(2\pi)^2}\mathrm{tr}\, e^{-ikx}[f(D_-D_+/M^2)\\ &\quad - f(D_+D_-/M^2)]e^{ikx},\end{aligned}$$

where Tr means a trace over all the states while tr is a trace over the layer and site indices or, equivalently, m, X, and even (odd) indices in Eq. (25).

The operator $\boldsymbol{\pi}$ acts on a plane wave to give $e^{-ikx}\boldsymbol{\pi}e^{ikx} = \hbar\boldsymbol{k} + \boldsymbol{\pi}$. Since $D_\pm$ contains at most first-order derivative terms, we can write

$$\begin{aligned}e^{-ikx}D_+e^{ikx} &= D_0|\boldsymbol{k}| + D_+,\\ e^{-ikx}D_-e^{ikx} &= D_0^\dagger|\boldsymbol{k}| + D_-,\end{aligned}$$

where D_0 is a c-number matrix and of zeroth order in $|\boldsymbol{k}|$, but may depend on a polar angle of $\boldsymbol{k}$. Since D_0 is a square matrix, it can be written in a singular value decomposition,

$$D_0 = U\Sigma V^\dagger,$$

with unitary matrices U,V and a diagonal matrix $\Sigma = \mathrm{diag}(\sqrt{\lambda_i})$ $(\lambda_i \geqslant 0)$.

The action of D_-D_+ on a plane wave is then described as

$$e^{-ikx}D_\mp D_\pm e^{ikx} = G_\pm k^2 + F_\pm,$$

where

$$\begin{aligned}G_+ &= D_0^\dagger D_0 = V\Sigma^2V^\dagger,\\ G_- &= D_0D_0^\dagger = U\Sigma^2U^\dagger,\end{aligned}$$

are c-number matrices of zeroth order in $|\boldsymbol{k}|$. $F_\pm$ are matrices including the operator $\boldsymbol{\pi}$, and up to first order of $|\boldsymbol{k}|$.

Having in mind that the ultraviolet behavior ($\hbar vk \sim M$) is important for the contribution of the D_-D_+ term to the chiral index, we obtain

$$\begin{aligned}&\mathrm{tr}\{e^{-ikx}f(D_-D_+/M^2)e^{ikx}\}\\ &\quad= \mathrm{tr}\{Vf(k^2\Sigma^2/M^2 + V^\dagger F_+V/M^2)V^\dagger\}\\ &\quad= \mathrm{tr}\{f(k^2\Sigma^2/M^2) + f'(k^2\Sigma^2/M^2)(V^\dagger F_+V)/M^2\}\\ &\qquad + O(M^{-4})\\ &\quad= \sum_i\{f(k^2\lambda_i/M^2) + f'(k^2\lambda_i/M^2)(V^\dagger F_+V)_{ii}/M^2)\}\\ &\qquad + O(M^{-4}).\end{aligned}$$

With a similar form for the D_+D_- term, the chiral index with $M\to\infty$ reduces to

$$\begin{aligned}\nu = \int d^2x \int \frac{d^2k}{(2\pi)^2}\sum_i f'(k^2\lambda_i/M^2)\\ \times (V^\dagger F_+V - U^\dagger F_-U)_{ii}/M^2. \qquad \text{(A2)}\end{aligned}$$

As argued in Sec. V, the Hamiltonian of multilayer graphene with $\Delta = 0$ is decomposed into block-diagonal form with effective monolayer and bilayer blocks labeled by m, and when the number of layers is odd, Δ always enters in the off-diagonal blocks. Then $G_\pm$ is block-diagonal because it is independent of Δ, and so U and V are. Therefore, although block off-diagonal terms in $F_\pm$ arise from Δ, they do not contribute to the sum of $(V^\dagger F_+V - U^\dagger F_-U)_{ii}$, and thus we only have to compute the chiral index for each block separately and add them up to obtain the overall chiral index.

Monolayer block ($m = 0$). Using the commutation relation $[\pi,\pi^\dagger] = -\xi 2\hbar eB$,

$$\begin{aligned}D_-D_+/v^2 &= \pi^\dagger\pi = \boldsymbol{\pi}^2 + \xi\hbar eB,\\ D_+D_-/v^2 &= \pi\pi^\dagger = \boldsymbol{\pi}^2 - \xi\hbar eB,\\ G_\pm &= \hbar^2v^2,\\ F_\pm &= v^2(\boldsymbol{\pi}^2 + 2\hbar\boldsymbol{k}\cdot\boldsymbol{\pi}) \pm \xi v^2\hbar eB.\end{aligned}$$

From Eq. (A2),

$$\begin{aligned}\nu &= \int d^2x \int \frac{d^2k}{(2\pi)^2} f'(\hbar^2v^2k^2/M^2)(2\xi v^2\hbar eB)/M^2\\ &= -\xi\Phi,\end{aligned}$$

where $\Phi = \int d^2x\, eB/h$ is the magnetic flux penetrating the system. When the magnetic field is uniform, this is the Landau-level degeneracy of the $n = 0$ Landau level, and its sign reflects that the level is assigned to $\psi_-(\psi_+)$ at the $K^+(K^-)$ valley.

Bilayer block ($m \neq 0$). For simplicity, we set $v = 1$ and $\lambda = 1$, and compensate it by redefining $M/v \to M$, $\lambda v_3/v \to v_3$, and $\lambda\gamma_1/v \to \gamma_1$. If we rewrite the block Hamiltonian Eq. (26) in an order of bases $|\phi_m^{(A,\mathrm{odd})}\rangle, |\phi_m^{(A,\mathrm{even})}\rangle, |\phi_m^{(B,\mathrm{even})}\rangle, |\phi_m^{(B,\mathrm{odd})}\rangle$ as

$$H = \begin{pmatrix}0 & D_-\\ D_+ & 0\end{pmatrix} = \begin{pmatrix}0 & 0 & v_3\pi & \pi^\dagger\\ 0 & 0 & \pi^\dagger & \gamma_1\\ v_3\pi^\dagger & \pi & 0 & 0\\ \pi & \gamma_1 & 0 & 0\end{pmatrix},$$

we have

$$\begin{aligned}D_-D_+ &= \begin{pmatrix}\boldsymbol{\pi}^2(1+v_3^2) & \gamma_1\pi^\dagger + v_3\pi^2\\ \gamma_1\pi + v_3(\pi^\dagger)^2 & \boldsymbol{\pi}^2 + \gamma_1^2\end{pmatrix}\\ &\quad + \xi\hbar eB\begin{pmatrix}1-v_3^2 & 0\\ 0 & 1\end{pmatrix},\\ D_+D_- &= \begin{pmatrix}\boldsymbol{\pi}^2(1+v_3^2) & \gamma_1\pi + v_3(\pi^\dagger)^2\\ \gamma_1\pi^\dagger + v_3\pi^2 & \boldsymbol{\pi}^2 + \gamma_1^2\end{pmatrix}\\ &\quad - \xi\hbar eB\begin{pmatrix}1-v_3^2 & 0\\ 0 & 1\end{pmatrix}.\end{aligned}$$

The action on the plane-wave basis is then given by

$$\begin{aligned}e^{-ikx}D_-D_+e^{ikx} &= G_+k^2 + \tilde{F} + F,\\ e^{-ikx}D_+D_-e^{ikx} &= (G_+k^2 + \tilde{F})^{\mathrm{T}} - F,\\ G_+ &= \hbar^2\begin{pmatrix}1+v_3^2 & v_3e^{2i\theta}\\ v_3e^{-2i\theta} & 1\end{pmatrix},\\ F &= \xi\hbar eB\begin{pmatrix}1-v_3^2 & 0\\ 0 & 1\end{pmatrix},\end{aligned}$$

where $\tilde{F}$ is a matrix including $\boldsymbol{\pi}$, of which the expression (not presented) is not important in the following argument.

With a relation $tr\, f(A) = \mathrm{tr}\, f(A^{\mathrm{T}})$, an explicit calculation of Eq. (A2) shows that

$$\begin{aligned}\nu &= \int d^2x \int \frac{d^2k}{(2\pi)^2} \sum_i f'(k^2\lambda_i/M^2) \\ &\quad \times [V^\dagger(\tilde{F}+F)V - (V^{\mathrm{T}})^\dagger(\tilde{F}^{\mathrm{T}}-F)V^{\mathrm{T}}]_{ii}/M^2 \\ &= \int d^2x \int \frac{d^2k}{(2\pi)^2} \sum_i f'(k^2\lambda_i/M^2)(2V^\dagger F V)_{ii}/M^2 \\ &= -\frac{1}{2\pi}\int d^2x \sum_i \frac{1}{\lambda_i}(V^\dagger F V)_{ii} \\ &= -\frac{1}{2\pi}\int d^2x\, \mathrm{tr}\,(G_+^{-1}F) = -2\xi\Phi.\end{aligned}$$

Thus, the chiral index of the bilayer block is twice that of the monolayer block, and inclusion of v_3 does not affect the result. This is naturally expected because the chiral index is a topological number and never changes in a continuous deformation.

If we combine these results for the monolayer and bilayer blocks noting the orders of the chiral bases for each block [Eq. (27)], we find that the chiral index for biased N (odd) -layered graphene is given by

$$\begin{aligned}n_+ - n_- &= (-1+2-2+2\ldots)\xi\Phi \\ &= \begin{cases} -\xi\Phi, & N = 4l+1, \\ +\xi\Phi, & N = 4l+3. \end{cases}\end{aligned}$$

This exactly coincides with Eq. (28), while the present argument is more general and valid for nonuniform magnetic field $B(x,y)$.

APPENDIX B: DERIVATION OF THE EDGE MODES FROM THE EFFECTIVE-MASS HAMILTONIAN

When the Hamiltonian is linear in $\boldsymbol{k}$, it is possible to obtain the edge state energies in the bulk gap by searching for the evanescent modes satisfying a boundary condition at the interface. We consider a $2N \times 2N$ Hamiltonian matrix $H(\hat{k}_x,\hat{k}_y)$ with $\hat{\boldsymbol{k}} = -i\boldsymbol{\nabla}$, and we assume it is linear in $\hat{\boldsymbol{k}}$. It is expressed as

$$H = A\hat{k}_y + B(\hat{k}_x), \tag{B1}$$

where A and B are $2N \times 2N$ matrices and A is independent of $\hat{k}_x$. We assume the system is periodic in x and we replace $\hat{k}_x$ with its eigenvalue k_x. H is regarded as a one-dimensional Hamiltonian with a parameter k_x. The Schrödinger equation, $H\boldsymbol{F}(y) = \varepsilon\boldsymbol{F}(y)$, is transformed to

$$\frac{\partial}{\partial y}\boldsymbol{F}(y) = iA^{-1}[-B(k_x)+\varepsilon]\boldsymbol{F}(y) \equiv M(k_x,\varepsilon)\boldsymbol{F}(y), \tag{B2}$$

with $M = iA^{-1}[-B(k_x)+\varepsilon]$. Let $\kappa^{(\alpha)}$ and $\boldsymbol{f}^{(\alpha)}(\alpha = 1,\ldots,2N)$ be the eigenvalues and right eigenvectors of the matrix $M(k_x,\varepsilon)$, The corresponding wave function becomes

$$\boldsymbol{F}^{(\alpha)}(y) = \exp(\kappa^{(\alpha)}y)\boldsymbol{f}^{(\alpha)}. \tag{B3}$$

Generally $\kappa^{(\alpha)}$ is a complex number, and the state is a bulk mode when $\kappa^{(\alpha)}$ is pure imaginary, and an evanescent mode otherwise. When the bulk spectrum of $H(k_x,k_y)$ is fully gapped at particular k_x, and ε is inside the gap, we have $2N$ evanescent modes with N modes of $\mathrm{Re}\,\kappa^{(\alpha)} > 0$ and another N modes of $\mathrm{Re}\,\kappa^{(\alpha)} < 0$. When we consider the half-infinite system in the region $y \geqslant 0$, an edge state localized near $y = 0$, if it exists, should be written as a linear combination of the states with $\mathrm{Re}\,\kappa^{(\alpha)} < 0$. When the indices $\alpha = 1,2,\ldots,N$ are assigned to the modes of $\mathrm{Re}\,\kappa^{(\alpha)} < 0$, it is written as

$$\boldsymbol{F}(y) = \sum_{\alpha=1}^{N} C^{(\alpha)} \exp(\kappa^{(\alpha)}y)\boldsymbol{f}^{(\alpha)}. \tag{B4}$$

The boundary condition at $y = 0$ for the wave function $\boldsymbol{F}$ is composed of N linear equations with respect to the $2N$-dimensional vector $\boldsymbol{F}(0)$. This is written as $D\boldsymbol{F}(0) = 0$, with D being an $N \times 2N$ constant matrix. For the trilayer graphene with a zigzag edge, for example, the boundary condition at $y = 0$ is $F_1(0) = F_3(0) = F_5(0) = 0$, so that D becomes

$$D = \begin{pmatrix} 1 & 0 & 0 & 0 & 0 & 0 \\ 0 & 0 & 1 & 0 & 0 & 0 \\ 0 & 0 & 0 & 0 & 1 & 0 \end{pmatrix}. \tag{B5}$$

By using Eq. (B4), the boundary condition is written as

$$X\begin{pmatrix} C^{(1)} \\ C^{(2)} \\ \vdots \\ C^{(N)} \end{pmatrix} = \begin{pmatrix} 0 \\ 0 \\ \vdots \\ 0 \end{pmatrix}, \tag{B6}$$

where $X = X(k_x,\varepsilon)$ is an $N \times N$ matrix defined by

$$X = D\left(\boldsymbol{f}^{(1)},\boldsymbol{f}^{(2)},\ldots,\boldsymbol{f}^{(N)}\right). \tag{B7}$$

The equation has a nontrivial solution when $\det X(k_x,\varepsilon) = 0$. The edge mode energy can be found by tracing $\det X(k_x,\varepsilon)$ throughout the energy gap, for each fixed k_x. When more than two edge modes are degenerate at the energy ε, the number of degeneracy is found by $N - \mathrm{rank}X(k_x,\varepsilon)$.

[1] J. McClure, Phys. Rev. **104**, 666 (1956).
[2] D. P. DiVincenzo and E. J. Mele, Phys. Rev. B **29**, 1685 (1984).
[3] G. W. Semenoff, Phys. Rev. Lett. **53**, 2449 (1984).
[4] T. Ando, J. Phys. Soc. Jpn. **74**, 777 (2005).
[5] N. H. Shon and T. Ando, J. Phys. Soc. Jpn. **67**, 2421 (1998).
[6] T. Ando, Y. Zheng, and H. Suzuura, J. Phys. Soc. Jpn. **71**, 1318 (2002).
[7] Y. Zheng and T. Ando, Phys. Rev. B **65**, 245420 (2002).
[8] V. P. Gusynin and S. G. Sharapov, Phys. Rev. Lett. **95**, 146801 (2005).
[9] K. Novoselov, A. Geim, S. Morozov, D. Jiang, M. Katsnelson, I. Grigorieva, S. Dubonos, and A. Firsov, Nature (London) **438**, 197 (2005).

[10]Y. Zhang, Y. W. Tan, H. L. Stormer, and P. Kim, Nature (London) **438**, 201 (2005).
[11]A. H. Castro Neto, F. Guinea, N. M. R. Peres, K. S. Novoselov, and A. K. Geim, Rev. Mod. Phys. **81**, 109 (2009).
[12]K. Novoselov, E. McCann, S. Morozov, V. Fal'ko, M. Katsnelson, U. Zeitler, D. Jiang, F. Schedin, and A. Geim, Nat. Phys. **2**, 177 (2006).
[13]T. Ohta, A. Bostwick, T. Seyller, K. Horn, and E. Rotenberg, Science **313**, 951 (2006).
[14]T. Ohta, A. Bostwick, J. McChesney, T. Seyller, K. Horn, and E. Rotenberg, Phys. Rev. Lett. **98**, 206802 (2007).
[15]E. V. Castro, K. S. Novoselov, S. V. Morozov, N. M. R. Peres, J. M. B. Lopes dos Santos, J. Nilsson, F. Guinea, A. K. Geim, and A. H. Castro Neto, Phys. Rev. Lett. **99**, 216802 (2007).
[16]J. Güttinger, C. Stampfer, F. Molitor, D. Graf, T. Ihn, and K. Ensslin, New J. Phys. **10**, 125029 (2008).
[17]M. Craciun, S. Russo, M. Yamamoto, J. Oostinga, A. Morpurgo, and S. Tarucha, Nat. Nanotech. **4**, 383 (2009).
[18]W. Zhu, V. Perebeinos, M. Freitag, and P. Avouris, Phys. Rev. B **80**, 235402 (2009).
[19]W. Bao, L. Jing, J. Velasco, Jr, Y. Lee, G. Liu, D. Tran, B. Standley, M. Aykol, S. B. Cronin, D. Smirnov, M. Koshino, E. McCann, M. Bockrath, and C. N. Lau, Nat. Phys. **7**, 948 (2011).
[20]T. Taychatanapat, K. Watanabe, T. Taniguchi, and P. Jarillo-Herrero, Nat. Phys. **7**, 621 (2011).
[21]E. McCann and V. I. Fal'ko, Phys. Rev. Lett. **96**, 086805 (2006).
[22]F. Guinea, A. H. Castro Neto, and N. M. R. Peres, Phys. Rev. B **73**, 245426 (2006).
[23]M. Koshino and T. Ando, Phys. Rev. B **73**, 245403 (2006).
[24]S. Latil and L. Henrard, Phys. Rev. Lett. **97**, 036803 (2006).
[25]B. Partoens and F. M. Peeters, Phys. Rev. B **74**, 075404 (2006).
[26]C. L. Lu, C. P. Chang, Y. C. Huang, R. B. Chen, and M. L. Lin, Phys. Rev. B **73**, 144427 (2006).
[27]M. Aoki and H. Amawashi, Solid State Commun. **142**, 123 (2007).
[28]M. Koshino and T. Ando, Phys. Rev. B **76**, 085425 (2007).
[29]M. Koshino and T. Ando, Phys. Rev. B **77**, 115313 (2008).
[30]M. Koshino and E. McCann, Phys. Rev. B **79**, 125443 (2009).
[31]M. Koshino and T. Ando, Solid State Commun. **149**, 1123 (2009).
[32]M. Koshino and E. McCann, Phys. Rev. B **83**, 165443 (2011).
[33]J. Slonczewski and P. Weiss, Phys. Rev. **109**, 272 (1958).
[34]J. McClure, Phys. Rev. **119**, 606 (1960).
[35]M. Dresselhaus and G. Dresselhaus, Adv. Phys. **51**, 1 (2002).
[36]E. McCann, Phys. Rev. B **74**, 161403 (2006).
[37]H. Min, B. Sahu, S. K. Banerjee, and A. H. MacDonald, Phys. Rev. B **75**, 155115 (2007).
[38]J. B. Oostinga, H. B. Heersche, X. Liu, A. F. Morpurgo, and L. M. K. Vandersypen, Nat. Mater. **7**, 151 (2008).
[39]M. Koshino, Phys. Rev. B **81**, 125304 (2010).
[40]E. V. Castro, N. M. R. Peres, J. M. B. Lopes dos Santos, A. H. Castro Neto, and F. Guinea, Phys. Rev. Lett. **100**, 026802 (2008).
[41]J. Jung, F. Zhang, Z. Qiao, and A. H. MacDonald, Phys. Rev. B **84**, 075418 (2011).
[42]S. Murakami, N. Nagaosa, and S. Zhang, Science **301**, 1348 (2003).
[43]C. Kane and E. Mele, Phys. Rev. Lett. **95**, 226801 (2005).
[44]W. K. Tse, Z. Qiao, Y. Yao, A. H. MacDonald, and Q. Niu, Phys. Rev. B **83**, 155447 (2011).
[45]Z. Qiao, J. Jung, Q. Niu, and A. MacDonald, Nano Lett. **11**, 3453 (2011).
[46]Z. Qiao, S. A. Yang, B. Wang, Y. Yao, and Q. Niu, Phys. Rev. B **84**, 035431 (2011).
[47]Z. Qiao, W.-K. Tse, H. Jiang, Y. Yao, and Q. Niu, Phys. Rev. Lett. **107**, 256801 (2011).
[48]Z. Qiao, X. Li, W.-K. Tse, H. Jiang, Y. Yao, and Q. Niu, arXiv:1211.3802 (unpublished).
[49]X. Li, Z. Qiao, J. Jung, and Q. Niu, Phys. Rev. B **85**, 201404 (2012).
[50]F. D. M. Haldane, Phys. Rev. Lett. **61**, 2015 (1988).
[51]M. Oshikawa, Phys. Rev. B **50**, 17357 (1994).
[52]R. Jackiw and C. Rebbi, Phys. Rev. D **16**, 1052 (1977).
[53]K. Fujikawa, Phys. Rev. Lett. **42**, 1195 (1979).
[54]K. Fujikawa and H. Suzuki, *Path Integrals and Quantum Anomalies* (Oxford University Press, Oxford, 2004).
[55]S. Ryu and Y. Hatsugai, Phys. Rev. Lett. **89**, 077002 (2002).
[56]A. P. Schnyder and S. Ryu, Phys. Rev. B **84**, 060504 (2011).
[57]T. Heikkilä and G. Volovik, JETP Lett. **93**, 59 (2011).
[58]A. A. Burkov, M. D. Hook, and L. Balents, Phys. Rev. B **84**, 235126 (2011).
[59]R. B. Laughlin, Phys. Rev. B **23**, 5632 (1981).
[60]M. Sadowski, G. Martinez, M. Potemski, C. Berger, and W. De Heer, Phys. Rev. Lett. **97**, 266405 (2006).
[61]Z. Jiang, E. Henriksen, L. Tung, Y. Wang, M. Schwartz, M. Han, P. Kim, and H. Stormer, Phys. Rev. Lett. **98**, 197403 (2007).
[62]T. Morimoto, M. Koshino, and H. Aoki, Phys. Rev. B **86**, 155426 (2012).